Front. Mech. Eng. 2020, 15(2): 256–264
https://doi.org/10.1007/s11465-019-0573-7

RESEARCH ARTICLE

Song ZHANG, Lelun WANG, Anze YI, Honggang GU, Xiuguo CHEN, Hao JIANG, Shiyuan LIU

Dynamic modulation performance of ferroelectric liquid crystal polarization rotators and Mueller matrix polarimeter optimization

Abstract A ferroelectric liquid crystal polarization rotator (FLCPR) has been widely used in polarization measurement due to its fast and stable modulation characteristics. The accurate characterization of the modulation performance of FLCPR directly affects the measurement accuracy of the instrument based on liquid crystal modulation. In this study, FLCPR is accurately characterized using a self-developed high-speed Stokes polarimeter. Strong linear and weak circular birefringence are observed during modulation processes, and all the optical parameters of FLCPR are dependent on driving voltage. A dual FLCPR-based Mueller matrix polarimeter is designed on the basis of the Stokes polarimeter. The designed polarimeter combines the advantages of the high modulation frequency of FLCPR and the ultrahigh temporal resolution of the fast polarization measurement system in the Stokes polarimeter. The optimal configuration of the designed polarizer is predicted in accordance with singular value decomposition. A simulated thickness measurement of a 24 nm standard SiO_2 thin film is performed using the optimal configuration. Results show that the relative error in thickness measurement caused by using the unsatisfactory modulation characteristics of FLCPR reaches up to −4.34%. This finding demonstrates the importance of the accurate characterization of FLCPR in developing a Mueller matrix polarizer.

Keywords ferroelectric liquid crystal polarization rotator (FLCPR), dual liquid crystal Mueller matrix polarizer, design and optimization

Received August 13, 2019; accepted September 22, 2019

Song ZHANG, Lelun WANG, Anze YI, Honggang GU, Xiuguo CHEN, Hao JIANG (✉), Shiyuan LIU
School of Mechanical Science and Engineering, Huazhong University of Science and Technology, Wuhan 430074, China
E-mail: hjiang@hust.edu.cn

1 Introduction

A polarimeter is a powerful tool that can determine the optical properties of a sample by measuring the change in polarization state of polarized light after it interacts with the sample. Given its advantages of high precision, noncontact, and high stability, a Mueller matrix polarimeter has been widely used in many fields, such as in semiconductor thin film structure and periodic nanostructure measurements [1–4], new material research [5,6], and biological and chemical engineering [7–10]. Compared with the traditional Mueller matrix polarimeter, the high temporal resolution Mueller matrix polarimeter based on liquid crystal modulation developed in recent years has gained increasing attention in the field of real-time measurement due to its advantages of having no mechanical rotating parts, high time resolution, and accurate and stable output of polarized light [11]. Furthermore, the most representative ferroelectric liquid crystal polarization rotator (FLCPR), which has ultrahigh modulation frequency, high purity linearly polarized light output, and high extinction ratio, has been widely used in rapid polarization measurements [12].

Many scholars have recently conducted detailed research on the construction and optimization of polarimeters based on liquid crystal polarization rotators. Ladstein et al. [13] designed and constructed the first near-infrared (NIR) spectroscopic Mueller matrix ellipsometer based on FLCPR using the eigenvalue calibration method. Garcia-Caurel et al. [14] developed fast spectroscopic measurements of a complete Mueller matrix with 1 nm resolution ranging from the visible to the NIR regions using a charge coupled device (CCD) array coupled to a dispersion grid. Peinado et al. [11] designed Stokes and Mueller polarimeters based on FLCPR panels. The work mentioned in the preceding references was performed by assuming ideal optical polarizing components, in which FLCPR is modeled as a uniaxial birefringent wave plate

with two stable optical axis orientations switchable by a squared electrical signal. However, azimuth deviation and retardance fluctuation occur during the use of FLCPR, reducing measurement accuracy. The resolution of a polarimeter is mostly limited by the time resolution of the detector, and the modulation performance of FLCPR cannot be fully demonstrated. Furthermore, the duration is in dozens of microseconds for several rapid processes, such as high-speed impact [15], laser transient heating [16], and molecular reaction [17]. However, the traditional Mueller matrix polarimeter with a temporal resolution of several tens of milliseconds cannot capture these rapid processes [18]. Therefore, FLCPR should be accurately characterized before constructing an instrument. Accordingly, a Mueller matrix polarimeter with high temporal resolution and based on FLCPRs should be developed.

The accurate characterization of the modulation performance of FLCPR directly affects the measurement accuracy of an FLCPR-based polarimeter. Therefore, we first used a self-developed high-speed Stokes polarimeter to accurately characterize the dynamic modulation performance of FLCPR. Then, a Mueller matrix polarimeter with dual FLCPRs was designed. The designed polarimeter combines the advantages of the high-frequency modulation characteristics of FLCPR and the high temporal resolution demodulation characteristics of division-of-amplitude methods. The configuration optimization of the designed polarimeter was obtained using the eigenvalue method. Lastly, the measurement error due to the undesired modulation characteristics of FLCPR in the standard SiO_2 film thickness measurement experiment was evaluated.

2 Modulation principle of FLCPR

FLCPR consists of two glass substrates coated with transparent indium tin oxide (ITO) as the conductive layer on one side of the glass surface. The surface of ITO was then coated with a layer of polyimide as the alignment layer. The middle of the two alignment layers was filled with ferroelectric liquid crystal molecules (FLCMs). Phase retardance can be modulated by controlling the distance of the intermediate [19]. The structure and modulation principle of FLCPR are illustrated in Fig. 1.

In general, FLCPR can be considered a wave plate with an optical axis along the direction of the FLCM director. A typical FLCPR utilizes the fast response characteristics of a ferroelectric liquid crystal material to control the switching of FLCMs between the two directions of the relative angle θ by changing the driving voltage applied to the ferroelectric liquid crystal optical shutter while maintaining the same retardance [20]. The most common configuration is FLCPR with a retardance of $\delta = 180°$ or $\delta = 90°$ (similar to a half-wave plate or a quart-wave plate) and a relative rotation angle of $\theta = 45°$. However, the set phase retardance is related to wavelength, and the aforementioned configuration is only effective at a specific design wavelength [21].

3 Characterization of FLCPR

To further understand the modulation performance of FLCPR and correctly use FLCPR, we must measure and characterize the orientation of FLCMs, the phase retardance δ, and the relative rotation angle θ prior to using FLCPR. We selected a 50.8 mm achromatic FLCPR (AFLCPR; FPA-200-1020) produced by Meadowlark Optics at a design wavelength of 1020 nm with a phase retardance of 180°. In contrast with ordinary FLCPR, AFLCPR consists of an FLCPR sandwiched between two half-wave plates with optical axes parallel to each other [22].

At present, FLCPR is generally placed between two polarizers whose optical axes are orthogonal to each other in existing methods for measuring the physical parameters of FLCPR [21], as shown in Fig. 2. The azimuth φ_1 of the first polarizer varies between 0° and 180°, and the azimuth φ_2 of the second polarizer is maintained at 90° relative to

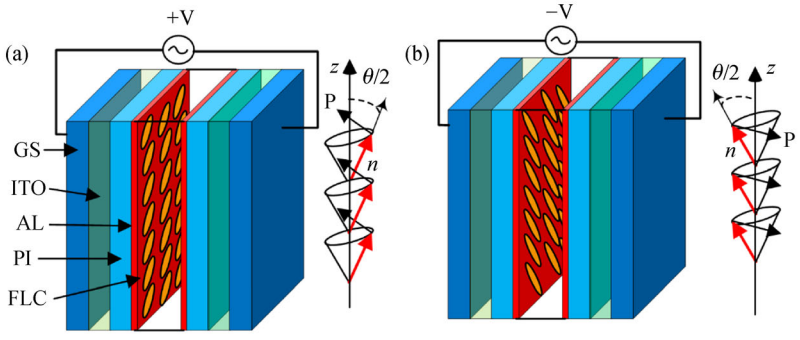

Fig. 1 Schematic of the structure and modulation principle of FLCPR: (a) and (b) at different driving voltages represent the two possible stable states in FLCPR. GS: Glass substrate; ITO: Thin conductive layer; PI: Polyimide layer; AL: Alignment layer; FLC: Ferroelectric liquid crystal; P: Spontaneous polarization; n: LC molecular director; and θ: Tilt angle of FLC.

φ_1. Then, the transmitted light intensities I_1 and I_2 at each azimuth are measured when FLCPR is under two stable states. We can calculate the retardance δ and the relative rotation angle θ of FLCPR using the variation law of the measured light intensities I_1 and I_2. However, polarizers P_1 and P_2 should be rotated multiple times, introducing measurement errors due to the rotation of optical elements. The entire process involves intermittent measurement, and the continuous modulation property of FLCPR cannot be observed. Moreover, FLCPR is considered a wave plate with a constant retardance and a relative rotation angle of 45° in this characterization method. However, all the physical parameters of FLCPR will change with the modulation signal instead of only the relative rotation angle changing in the described characterization method. In addition, we found that FLCPR not only exhibits linear birefringence (LB) but also circular birefringence (CB) during modulation.

To compensate for the shortcomings of existing characterization methods, we propose a characterization model based on the Mueller matrix form that can simultaneously characterize the LB and CB of FLCPR. This model can be expressed as Eq. (1). All the optical parameters of FLCPR are dependent on driving voltage in the proposed characterization model.

$$\boldsymbol{M}_{\mathrm{AFLCPR}} = A\cdot\boldsymbol{M}_{\mathrm{HWP}}(\beta,\delta_{\mathrm{HWP}})\cdot\boldsymbol{M}_{\mathrm{FLCPR}}(\alpha,\delta_{\mathrm{FLCPR}},\chi)\cdot\boldsymbol{M}_{\mathrm{HWP}}(\beta,\delta_{\mathrm{HWP}}), \tag{1}$$

where $\boldsymbol{M}_{\mathrm{AFLCPR}}$ is the Mueller matrix of AFLCPR, $\boldsymbol{M}_{\mathrm{HWP}}$ is the Mueller matrix of half-wave plates, and $\boldsymbol{M}_{\mathrm{FLCPR}}$ is the Mueller matrix of FLCPR [23–25]. A is the relative transmittance of FLCPR, β is the azimuth of the half-wave plates, δ_{HWP} is the retardance of the half-wave plates, α is the azimuth of FLCPR, δ_{FLCPR} is the retardance of FLCPR, and γ is the optical rotation angle of FLCPR. To simplify the expression, we define $\chi = \alpha + \gamma$.

$$\boldsymbol{M}_{\mathrm{HWP}} = \begin{pmatrix} 1 & 0 & 0 & 0 \\ 0 & \cos(4\beta)\sin(\delta_{\mathrm{HWP}}/2)^2 + \cos(\delta_{\mathrm{HWP}}/2)^2 & \sin(4\beta)\sin(\delta_{\mathrm{HWP}}/2)^2 & -\sin(2\beta)\sin(\delta_{\mathrm{HWP}}) \\ 0 & -\sin(4\beta)\sin(\delta_{\mathrm{HWP}}/2)^2 & -\cos(4\beta)\sin(\delta_{\mathrm{HWP}}/2)^2+\cos(\delta_{\mathrm{HWP}}/2)^2 & \cos(2\beta)\sin(\delta_{\mathrm{HWP}}) \\ 0 & \sin(2\beta)\sin(\delta_{\mathrm{HWP}}) & \cos(2\beta)\sin(\delta_{\mathrm{HWP}}) & \cos(\delta_{\mathrm{HWP}}) \end{pmatrix}, \tag{2}$$

$$\boldsymbol{M}_{\mathrm{FLCPR}} = \begin{pmatrix} 1 & 0 & 0 & 0 \\ 0 & \cos(2\chi)\cos(2\alpha)-\sin(2\chi)\sin(2\alpha)\cos(\delta_{\mathrm{FLCPR}}) & \sin(2\chi)\cos(2\alpha)-\cos(2\chi)\sin(2\alpha)\cos(\delta_{\mathrm{FLCPR}}) & -\sin(2\alpha)\sin(\delta_{\mathrm{FLCPR}}) \\ 0 & \cos(2\chi)\sin(2\alpha)-\sin(2\chi)\cos(2\alpha)\cos(\delta_{\mathrm{FLCPR}}) & \cos(2\chi)\cos(2\alpha)\cos(\delta_{\mathrm{FLCPR}})+\sin(2\chi)\sin(2\alpha) & \cos(2\alpha)\sin(\delta_{\mathrm{FLCPR}}) \\ 0 & \sin(2\chi)\sin(\delta_{\mathrm{FLCPR}}) & -\cos(2\chi)\sin(\delta_{\mathrm{FLCPR}}) & \cos(\delta_{\mathrm{FLCPR}}) \end{pmatrix}. \tag{3}$$

To measure the continuous modulation characteristics of FLCPR in real time, the self-developed Stokes polarimeter with six parallel detection channels is used in the dynamic characterization experiments of FLCPR. Applying the concept of modular design [26], the Stokes polarimeter consists of three parts: A polarization state generator (PSG), a sample stage, and a fast polarization measurement system (FPMS), as shown schematically in Fig. 3. In the

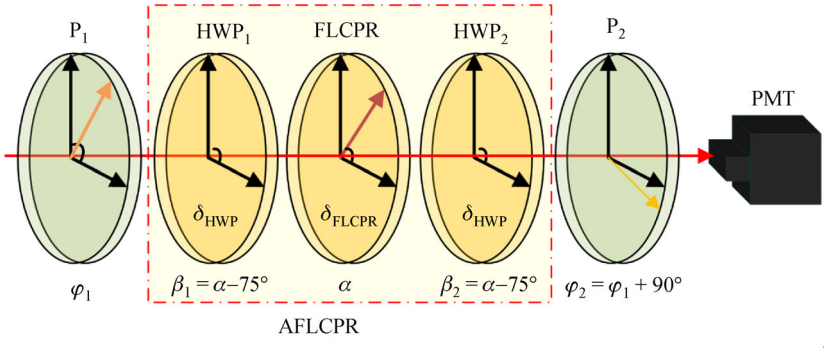

Fig. 2 Schematic of FLCPR measurement methods in the literature. P: Polarizer; HWP: Half-wave plate; FLCPR: Normal ferroelectric liquid crystal polarization rotator; AFLCPR: Achromatic ferroelectric liquid crystal polarization rotator; PMT: Photomultiplier tube.

PSG part, the light source used is a 5 mW red (632.8 nm) He–Ne laser (THORLABS). The PSG can achieve the light output of an arbitrary polarization state with the combination of linear polarizers and wave plates. FPMS based on the principle of spatial division of amplitude can detect all the Stokes parameters of the probing light in several nanoseconds. Moreover, the polarimeter can be used under various measurement configurations with a rotatable base and a flexible sample stage, which can be composed of different displacement and tilt platforms [27–29]. Lastly, the influence of temperature is not considered in our experiments because the experiments are performed in a clean room with constant temperature and humidity.

To illustrate the continuous modulation characteristics of FLCPR, a square wave signal with a modulation period of 1 s and an amplitude of 10 voltage peak-peak is used as the modulation signal. Several results are shown in Fig. 4, in which all the optical parameters of FLCPR are dependent on driving voltage. Furthermore, we confirm the LB property and weak CB property during the modulation processes of FLCPR. To clearly illustrate the variation of the related optical parameters, we extract the optical parameters of FLCPR in two different stable states at time points 0.5 and 1 s. The extracted results are provided in Table 1.

The extracted results presented in Table 1 show that the relative rotation angle is 46.17°, which is 1.17° larger than the ideal configuration of 45°. Furthermore, the retardance is 262.20° and 260.40° in the two stable states. The difference between the two states is 1.80°. Given that the

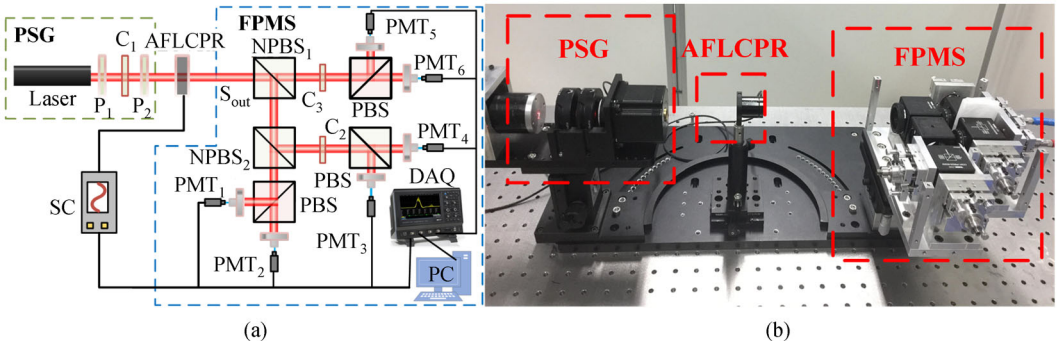

Fig. 3 Six-channel Stokes polarimeter. (a) Light path diagram. P_1 and P_2: Polarizers; C_1 and C_3: Quart-wave plate; C_2: Half-wave plate; $NPBS_1$: 70:30 (R:T) non-polarizing beam splitter; $NPBS_2$: 50:50 (R:T) non-polarizing beam splitter; PBS: Polarization beam splitter; DAQ: Oscilloscope; PC: Personal computer; SC: Signal controller; PMT: Photomultiplier tube. (b) Self-developed Stokes polarimeter prototype.

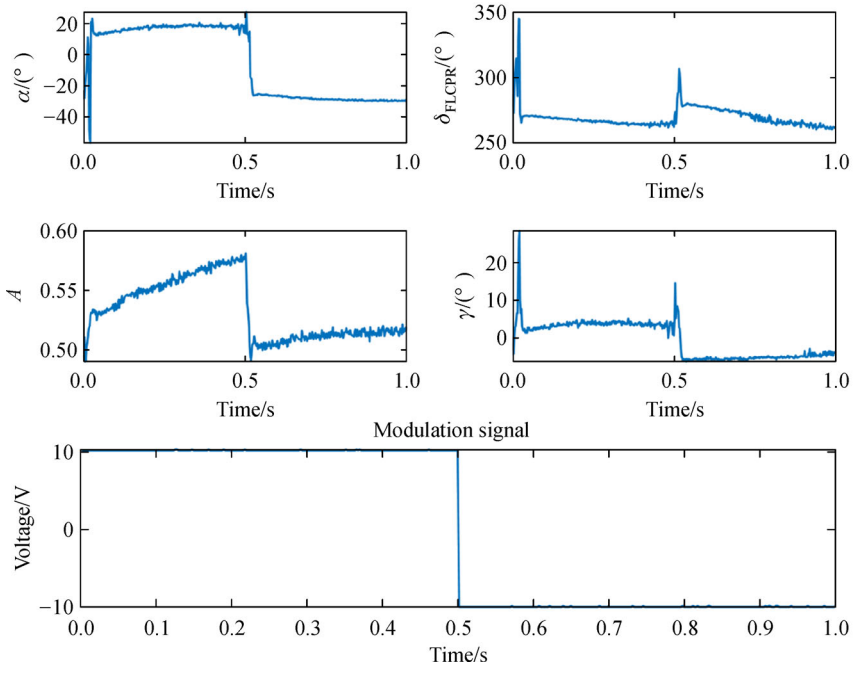

Fig. 4 Real-time measurement of FLCPR with the self-developed Stokes polarimeter.

Table 1 Optical parameters extracted for FLCPR

Time point	α/(°)	δ_{FLCPR}/(°)	A	γ/(°)
0.5 s	16.30	262.20	0.5745	2.37
1 s	−29.87	260.40	0.5122	−3.75
Δ	46.17	1.80	0.0630	5.12

designed wavelength of AFLCPR is 1020 nm, the relative transmittance is only approximately 0.5 under the wavelength of 633 nm. Furthermore, the relative transmittance is not constant during the dynamic measurement experiment. The relative transmittance changes by 0.063 in the two different states of FLCPR. In addition, the optical rotation angle of FLCPR varies within the range of ±4° between the two stable states, demonstrating the existence of the weak CB property in the modulation process of FLCPR. In summary, the aforementioned extracted results confirm the correctness of the proposed characterization model and inference. That is, FLCPR exhibits not only the LB property but also the weak CB property in the modulation processes. All the optical parameters of FLCPR vary with driving voltage.

4 Optimization of the dual FLCPR-based Mueller matrix polarimeter

At present, the self-developed high-speed Stokes polarimeter, which has a temporal resolution of several nanoseconds, can simultaneously measure all the Stokes vectors of the probe light. Given that the polarizer is rotated by mechanical components to output polarized light with different polarization states, the temporal resolution of the Mueller matrix measurement remains low. Therefore, by combining the high modulation frequency of FLCPR and the ultrahigh temporal resolution of FPMS, we design a Mueller matrix polarimeter with dual FLCPRs based on the self-developed Stokes polarimeter, as shown in Fig. 5. In particular, two FLCPRs with a retardance of 90° and 180° at the design wavelength of 633 nm are added to the original polarization generator, and the other parts remain unchanged. The temporal resolution of the Mueller matrix measurement is no longer limited by the temporal resolution of the detector but primarily limited by the modulation frequency of FLCPRs. The design scheme is expected to achieve sub-millisecond temporal resolution in Mueller matrix measurement.

To identify all the 16 elements of the sample Mueller matrix, the designed Mueller matrix polarimeter should output light with at least four linearly independent polarization states. The measurement matrix $\boldsymbol{B}$ of the Mueller matrix polarimeter, which consists of intensity detected by six photomultiplier tubes (PMTs), can be generally represented by multiplying the modulation matrix $\boldsymbol{W}$ of the polarization generator, the sample Muller matrix $\boldsymbol{M}$, and the demodulation matrix $\boldsymbol{A}$ of the analyzer system [13,30], as shown in Eq. (4).

$$\boldsymbol{B}=[I_1 \quad I_2 \quad I_3 \quad I_4 \quad I_5 \quad I_6]^{\mathrm{T}} = \boldsymbol{AMW}, \tag{4}$$

where the column vector of $\boldsymbol{W}$ consists of the Stokes vector of incident light, as shown in Eq. (5).

$$\boldsymbol{S}_1 = \boldsymbol{R}(-\alpha_2)\boldsymbol{M}_{\mathrm{re}}(\delta_{\mathrm{FLCPR}_2})\boldsymbol{R}(\alpha_2)\boldsymbol{R}(-\alpha_1)\boldsymbol{M}_{\mathrm{re}}(\delta_{\mathrm{FLCPR}_1}) \cdot\boldsymbol{R}(\alpha_1)\boldsymbol{R}(-\theta_{\mathrm{p}})\boldsymbol{M}_{\mathrm{p}}\boldsymbol{R}(\theta_{\mathrm{p}})[1 \quad 0 \quad 0 \quad 1]^{\mathrm{T}}, \tag{5a}$$

$$\boldsymbol{S}_2 = \boldsymbol{R}(-\alpha_2)\boldsymbol{M}_{\mathrm{re}}(\delta_{\mathrm{FLCPR}_2})\boldsymbol{R}(\alpha_2)\boldsymbol{R}(-\alpha_1-45°) \cdot\boldsymbol{M}_{\mathrm{re}}(\delta_{\mathrm{FLCPR}_1})\boldsymbol{R}(\alpha_1+45°) \cdot\boldsymbol{R}(-\theta_{\mathrm{p}})\boldsymbol{M}_{\mathrm{p}}\boldsymbol{R}(\theta_{\mathrm{p}})[1 \quad 0 \quad 0 \quad 1]^{\mathrm{T}}, \tag{5b}$$

$$\boldsymbol{S}_3 = \boldsymbol{R}(-\alpha_2-45°)\boldsymbol{M}_{\mathrm{re}}(\delta_{\mathrm{FLCPR}_2})\boldsymbol{R}(\alpha_2+45°)\boldsymbol{R}(-\alpha_1) \cdot\boldsymbol{M}_{\mathrm{re}}(\delta_{\mathrm{FLCPR}_1})\boldsymbol{R}(\alpha_1) \cdot\boldsymbol{R}(-\theta_{\mathrm{p}})\boldsymbol{M}_{\mathrm{p}}\boldsymbol{R}(\theta_{\mathrm{p}})[1 \quad 0 \quad 0 \quad 1]^{\mathrm{T}}, \tag{5c}$$

$$\boldsymbol{S}_4 = \boldsymbol{R}(-\alpha_2-45°)\boldsymbol{M}_{\mathrm{re}}(\delta_{\mathrm{FLCPR}_2})\boldsymbol{R}(\alpha_2+45°) \cdot\boldsymbol{R}(-\alpha_1-45°)\boldsymbol{M}_{\mathrm{re}}(\delta_{\mathrm{FLCPR}_1})\boldsymbol{R}(\alpha_1+45°) \cdot\boldsymbol{R}(-\theta_{\mathrm{p}})\boldsymbol{M}_{\mathrm{p}}\boldsymbol{R}(\theta_{\mathrm{p}})[1 \quad 0 \quad 0 \quad 1]^{\mathrm{T}}, \tag{5d}$$

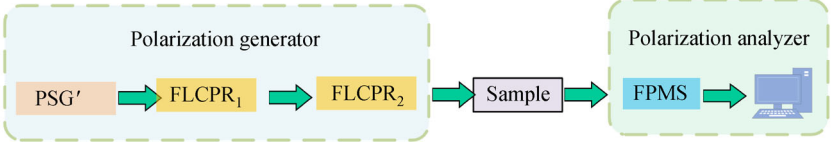

Fig. 5 Schematic of the Mueller matrix polarimeter based on dual FLCPRs.

$$\boldsymbol{W}(\alpha_1,\ \alpha_2,\ \theta_p)=[\boldsymbol{S}_1 \quad \boldsymbol{S}_2 \quad \boldsymbol{S}_3 \quad \boldsymbol{S}_4], \tag{5e}$$

where $\delta_{\mathrm{FLCPR}_1}$ and $\delta_{\mathrm{FLCPR}_2}$ are the retardance of the two FLCPRs, and $\delta_{\mathrm{FLCPR}_1}=90°$ and $\delta_{\mathrm{FLCPR}_2}=180°$, α_1 and α_2 are the azimuths of the two FLCPRs, θ_p is the azimuth of the polarizer P_2, $\boldsymbol{M}_{re}$ is the Mueller matrix of the retarder, and $\boldsymbol{R}$ is the rotation matrix.

In FPMS, two non-polarizing beam splitters (NPBSs) and three polarizing beam splitters (PBSs) divide the input light into six branch lights. A linear relationship exists between the first Stokes vector component $\boldsymbol{S}(0)$ and light intensity. Therefore, the demodulation matrix $\boldsymbol{A}$ of FPMS consists of the first-row vector of the Mueller matrix of the six branch lights.

$$\boldsymbol{a}_1=[1\quad 0\quad 0\quad 0]\cdot\boldsymbol{\Lambda}_{\mathrm{PBS}}\cdot\boldsymbol{\Gamma}_{\mathrm{NPBS55}}\cdot\boldsymbol{\Lambda}_{\mathrm{NPBS73}}, \tag{6a}$$

$$\boldsymbol{a}_2=[1\quad 0\quad 0\quad 0]\cdot\boldsymbol{\Gamma}_{\mathrm{PBS}}\cdot\boldsymbol{\Gamma}_{\mathrm{NPBS55}}\cdot\boldsymbol{\Lambda}_{\mathrm{NPBS73}}, \tag{6b}$$

$$\boldsymbol{a}_3=[1\quad 0\quad 0\quad 0]\cdot\boldsymbol{\Lambda}_{\mathrm{PBS}}\cdot[\boldsymbol{R}(-\alpha_{c2})\cdot\boldsymbol{M}_{re}(\delta_{c2})\cdot\boldsymbol{R}(\alpha_{c2})]\cdot\boldsymbol{\Lambda}_{\mathrm{NPBS55}}\cdot\boldsymbol{\Lambda}_{\mathrm{NPBS73}}, \tag{6c}$$

$$\boldsymbol{a}_4=[1\quad 0\quad 0\quad 0]\cdot\boldsymbol{\Gamma}_{\mathrm{PBS}}\cdot[\boldsymbol{R}(-\alpha_{c2})\cdot\boldsymbol{M}_{re}(\delta_{c2})\cdot\boldsymbol{R}(\alpha_{c2})]\cdot\boldsymbol{\Lambda}_{\mathrm{NPBS55}}\cdot\boldsymbol{\Lambda}_{\mathrm{NPBS73}}, \tag{6d}$$

$$\boldsymbol{a}_5=[1\quad 0\quad 0\quad 0]\cdot\boldsymbol{\Lambda}_{\mathrm{PBS}}\cdot[\boldsymbol{R}(-\alpha_{c3})\cdot\boldsymbol{M}_{re}(\delta_{c3})\cdot\boldsymbol{R}(\alpha_{c3})]\cdot\boldsymbol{\Gamma}_{\mathrm{NPBS73}}, \tag{6e}$$

$$\boldsymbol{a}_6=[1\quad 0\quad 0\quad 0]\cdot\boldsymbol{\Gamma}_{\mathrm{PBS}}\cdot[\boldsymbol{R}(-\alpha_{c3})\cdot\boldsymbol{M}_{re}(\delta_{c3})\cdot\boldsymbol{R}(\alpha_{c3})]\cdot\boldsymbol{\Gamma}_{\mathrm{NPBS73}}, \tag{6f}$$

$$\boldsymbol{A}(\alpha_{c2},\ \alpha_{c3})=[\boldsymbol{a}_1 \quad \boldsymbol{a}_2 \quad \boldsymbol{a}_3 \quad \boldsymbol{a}_4 \quad \boldsymbol{a}_5 \quad \boldsymbol{a}_6]^{\mathrm{T}}, \tag{6g}$$

where $\boldsymbol{\Lambda}$ and $\boldsymbol{\Gamma}$ represent the reflection and transmission matrices, respectively, $\boldsymbol{M}_i$ ($i=C_2$, C_3, PBS, NPBS73, NPBS55) is the Mueller matrix of the corresponding optical elements, α_{c2} and α_{c3} are the azimuth of the wave plates C_2 and C_3 and can vary between 0° and 360°. The Mueller matrices of PBSs and NPBSs are obtained in the *in situ* calibration process [27].

To promote noise immunity and reduce the error caused by the matrix operation, we perform the configuration optimization of the designed Muller matrix polarimeter by defining a merit, called a condition number, which can be used to assess the noise immunity of the polarimeter. The condition number $c(\boldsymbol{X})$ of a matrix $\boldsymbol{X}$ is equal to the ratio of the largest over the smallest of the singular values of $\boldsymbol{X}$ [31,32]. Therefore, we have to minimize the values of $c(\boldsymbol{A})$ and $c(\boldsymbol{W})$ to find the optimized configuration of the designed polarimeter.

In the Mueller matrix polarimeter with dual FLCPRs, the azimuth θ_p of the polarizer P_2, and the azimuths α_1 and α_2 of the two FLCPRs are adjustable in the polarization generator, and the azimuths α_{c2} and α_{c3} of the wave plates C_2 and C_3 are adjustable in FPMS. Therefore, the configuration of the designed polarimeter aims to essentially find a set of (α_1, α_2, θ_p) and (α_{c2}, α_{c3}) to minimize $c(\boldsymbol{W})$ and $c(\boldsymbol{A})$. The physical parameters of FLCPR change minimally based the measurement results of ALFCPR. To simplify the configuration procedure, all configuration optimization processes will be conducted in the ideal state of FLCPR. Thus, the relative rotation angle of FLCPR is 45°, the relevant physical parameters remain unchanged in two states, and the CB effect is neglected. Using the configuration optimization method based on a conditional number, we optimize the configuration of PSG and FPMS within the range of (α_1, α_2, θ_p)∈[0°, 90°] and (α_{c2}, α_{c3})∈[0°, 180°]. The results are presented in Figs. 6 and 7.

As shown in the optimization results of PSG in Fig. 6(a), the azimuth of FLCPR_2 barely affects the value of $c(\boldsymbol{W})$. Then, we find the minimum value of $c(\boldsymbol{W})$ with the pair (α_2, θ_p). The results are presented in Fig. 6(b). When the azimuths of polarizer P_2 and FLCPR_1 satisfy the relationship in Eq. (7a), $c(\boldsymbol{W})$ will reach the minimum value of 2.0000. The polarized light produced by PSG is linearly

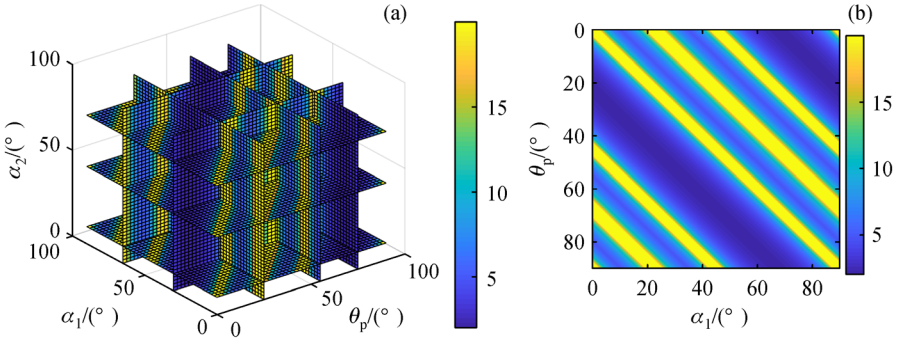

Fig. 6 Diagram of the configuration optimization of PSG: (a) Relationship between (α_1, α_2, θ_p) and $c(\boldsymbol{W})$; (b) relationship between (α_1, θ_p) and $c(\boldsymbol{W})$. The value of $c(\boldsymbol{W})$ spans from two to infinity. Thus, the area with $c(\boldsymbol{W})>20$ is displayed in the same color to achieve a clear depiction of the position of the smallest $c(\boldsymbol{W})$.

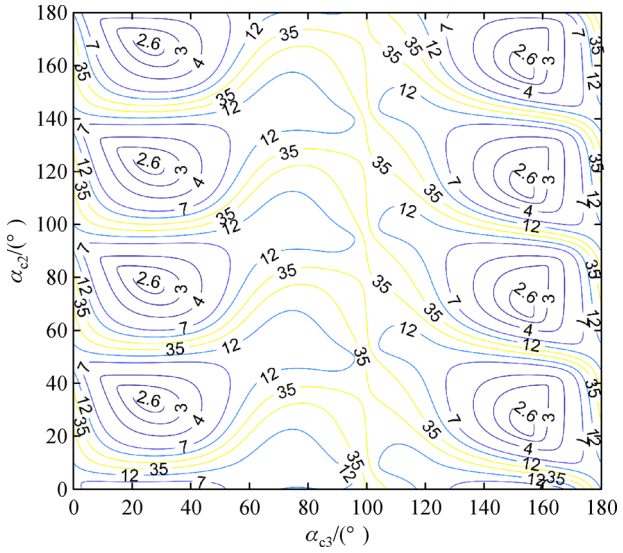

Fig. 7 Diagram of the configuration optimization of FPMS. Relationship between (α_{c2}, α_{c3}) and $c(\boldsymbol{A})$.

correlated when the azimuths of polarizer P_2 and $FLCPR_1$ satisfy the relationship in Eq. (7b). The value of $c(\boldsymbol{W})$ is infinite. Therefore, we should prevent PSG from outputting polarized light near this configuration.

$$\theta_p = \alpha_1 + 22.5° + k\cdot 90° \ (k \in Z), \tag{7a}$$

$$\theta_p = \alpha_1 + l\cdot 22.5° + m\cdot 90° \ (l = 0,\ 2,\ 3;\ m \in Z). \tag{7b}$$

The optimization results of FPMS shown in Fig. 7 indicate that $c(\boldsymbol{A})$ reaches the minimum value of 2.4796 when α_{c2} and α_{c3} satisfy Eq. (8). The azimuths α_{c2} and α_{c3} of the wave plates in FPMS take the values near the recommended value to enhance noise immunity and improve the stability of the polarimeter.

$$(\alpha_2, \alpha_3) = (25.4° + q\cdot 45°, 32.7°) \ (q \in Z), \tag{8a}$$

$$(\alpha_2, \alpha_3) = (25.4° + q\cdot 45°, 153.7°) \ (q \in Z). \tag{8b}$$

5 Evaluation of measurement errors

The retardance, which remains unchanged during the modulation process, and the relative rotation angle of FLCPR are measured in advance in the existing literatures. However, all the optical parameters of FLCPR vary with driving voltage in accordance with the measurement results of AFLCPR. Errors caused by changes in transmittance can be avoided by normalizing the measured light intensity. Weak CB effects exert negligible effects on the measurement results. However, retardance varies by approximately ±2° between the two stable states. If we disregard the change in retardance similar to that in the literature, then the measurement accuracy of the instrument will be reduced. To diminish the influence of the undesired modulation performance of FLCPR on measurement accuracy, the measurement error caused by the fluctuation of retardance should be evaluated.

For example, we simulate the thickness measurement error caused by the fluctuation of the retardance in the thickness measurement experiment of a 24 nm standard SiO_2 film sample. The simulation experiment is performed under the optimal configuration obtained in Section 4, i.e., (α_1, α_2, θ_p) = (22.5°, 45°, 45°) and (α_{c2}, α_{c3}) = (25.4°, 32.7°), with an incident angle of 51° in the reflection measurement mode. When the modulation matrix $\boldsymbol{W}$ and the demodulation matrix $\boldsymbol{A}$ are determined through the calibration process, the ellipsometry parameters (ψ, Δ) can be obtained using Eq. (9).

$$\boldsymbol{M}(\psi, \Delta) = \boldsymbol{A}^{-1}\boldsymbol{B}\boldsymbol{W}^{-1}. \tag{9}$$

The thickness of the film can be calculated from the measured ellipsometry parameters via library matching operation. Given that the measured matrix $\boldsymbol{B}$ is obtained in real time, thickness variation can be determined using the designed Mueller matrix polarimeter. The thickness measurement error of the simulation experiment is shown in Fig. 8.

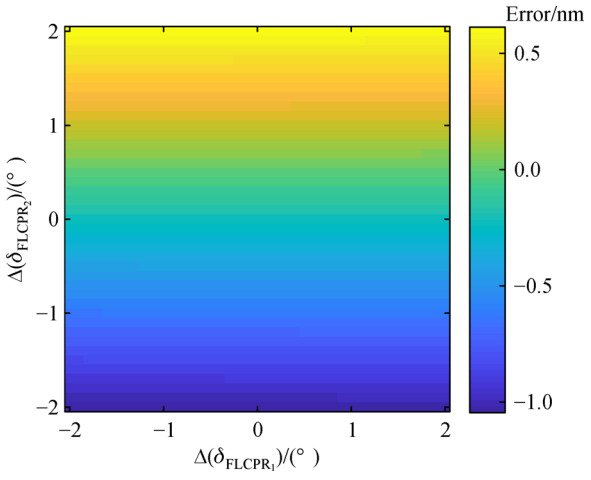

Fig. 8 Thickness measurement error in SiO_2 film measurement caused by the retardance change of FLCPR.

The simulation results shown in Fig. 8 indicate that the maximum thickness measurement error is −1.045 nm in the thickness measurement experiment of the 24 nm standard SiO_2 film sample, indicating that the relative measurement error reaches up to −4.35%. However, the retardance fluctuation of $FLCPR_1$ exerts minimal effect on thickness measurement. The retardance fluctuation of

$FLCPR_2$ is the primary factor that causes the thickness measurement error. Therefore, a change in the retardance of FLCPR must be accurately measured when developing FLCPR-based polarimeters to reduce errors caused by the unsatisfactory modulation property of FLCPR.

6 Conclusions

The accurate characterization of the modulation performance of FLCPR directly affects the measurement accuracy of polarimeters based on FLCPRs. In this work, the accurate characterization of FLCPR using a self-developed high-speed Stokes polarimeter proves that all the optical parameters of FLCPR are dependent on driving voltage. Furthermore, FLCPR exhibits not only the LB property but also the weak CB property. Then, we design a Mueller matrix polarimeter with dual FLCPRs based on the self-developed Stokes polarimeter. The designed polarimeter combines the advantages of the high modulation frequency of FLCPR and the ultrahigh temporal resolution of FPMS. Furthermore, we obtain the optimal configuration of the designed polarimeter by minimizing the number of conditions. Lastly, we evaluate the measurement error caused by the fluctuation of retardance in the simulated thickness measurement of a 24 nm standard SiO_2 film sample under optimal configuration. The maximum relative thickness measurement error of -4.35% indicates that the retardance change between the two stable states of FLCPR is crucial.

Acknowledgements This work was funded by the National Natural Science Foundation of China (Grant Nos. 51575214, 51525502, 51975232, 51727809, and 51805193), the National Key Research and Development Plan (Grant No. 2017YFF0204705), the Natural Science Foundation of Hubei Province of China (Grant No. 2018CFA057), and the National Science and Technology Major Project of China (Grant No. 2017ZX02101006-004).

References

1. Dmitruk N, Borkovskaya O Y, Mayeva O, et al. Polarization-sensitive photocurrents of metal-semiconductor structures with flat and microrelief interfaces. Microelectronics Journal, 1996, 27(1): 37–42
2. Liu S, Chen X, Zhang C. Development of a broadband Mueller matrix ellipsometer as a powerful tool for nanostructure metrology. Thin Solid Films, 2015, 584: 176–185
3. Arteaga O, Maoz B M, Nichols S, et al. Complete polarimetry on the asymmetric transmission through subwavelength hole arrays. Optics Express, 2014, 22(11): 13719–13732
4. Veis M, Antos R. Advances in optical and magnetooptical scatterometry of periodically ordered nanostructured arrays. Journal of Nanomaterials, 2013, 2013: 621531
5. Arteaga O, Kahr B. Mueller matrix polarimetry of bianisotropic materials. Journal of the Optical Society of America. B, Optical Physics, 2019, 36(8): F72–F83
6. Samim M, Krouglov S, James D F, et al. Characterization of heterogeneous media using nonlinear Stokes–Mueller polarimetry. Journal of the Optical Society of America. B, Optical Physics, 2016, 33(12): 2617–2625
7. Chue-Sang J, Gonzalez M, Pierre A, et al. Optical phantoms for biomedical polarimetry: A review. Journal of Biomedical Optics, 2019, 24(3): 030901
8. Fedick P W, Bain R M, Bain K, et al. Chiral analysis by tandem mass spectrometry using the kinetic method, by polarimetry, and by 1H NMR spectroscopy. Journal of Chemical Education, 2017, 94 (9): 1329–1333
9. Ghosh N, Soni J, Wood M, et al. Mueller matrix polarimetry for the characterization of complex random medium like biological tissues. Pramana-Journal of Physics, 2010, 75(6): 1071–1086
10. Bueno J M, Campbell M C. Confocal scanning laser ophthalmoscopy improvement by use of Mueller-matrix polarimetry. Optics Letters, 2002, 27(10): 830–832
11. Peinado A, Lizana A, Campos J. Optimization and tolerance analysis of a polarimeter with ferroelectric liquid crystals. Applied Optics, 2013, 52(23): 5748–5757
12. Bailey J, Kedziora-Chudczer L, Cotton D V, et al. A high-sensitivity polarimeter using a ferro-electric liquid crystal modulator. Monthly Notices of the Royal Astronomical Society, 2015, 449(3): 3064–3073
13. Ladstein J, Stabo-Eeg F, Garcia-Caurel E, et al. Fast near-infra-red spectroscopic Mueller matrix ellipsometer based on ferroelectric liquid crystal retarders. Physica Status Solidi. C, Current Topics in Solid State Physics, 2008, 5(5): 1097–1100
14. Garcia-Caurel E, De Martino A, Drevillon B. Spectroscopic Mueller polarimeter based on liquid crystal devices. Thin Solid Films, 2004, 455–456: 120–123
15. Kinslow R. High-Velocity Impact Phenomena. 1st ed. New York: Academic Press, 2012, 105–155
16. Tang D W, Zhou B L, Cao H, et al. Thermal stress relaxation behavior in thin films under transient laser-pulse heating. Journal of Applied Physics, 1993, 73(8): 3749–3752
17. Levine R D. Molecular Reaction Dynamics. Cambrideg: Cambridge University Press, 2005, 334–353
18. Collins R, Koh J. Dual rotating-compensator multichannel ellipsometer: Instrument design for real-time Mueller matrix spectroscopy of surfaces and films. Journal of the Optical Society of America. A, Optics, Image Science, and Vision, 1999, 16(8): 1997–2006
19. Babilotte P, Nunes Henrique Silva V, Sathaye K, et al. Twisted ferroelectric liquid crystals dynamic behaviour modification under electric field: A Mueller matrix polarimetry approach using birefringence. Journal of Applied Physics, 2014, 115(3): 034906
20. Wang L, Melnik R, Lv F. Stress induced polarization switching and coupled hysteretic dynamics in ferroelectric materials. Frontiers of Mechanical Engineering, 2011, 6(3): 287–291
21. Martínez A, Beaudoin N, Moreno I, et al. Optimization of the contrast ratio of a ferroelectric liquid crystal optical modulator. Journal of Optics, 2006, 8(11): 1013–1018
22. Rebolledo N A, Kyle D C, Phipps D P. Achromatic ferroelectric liquid crystal polarization rotator. Proceedings Volume 10655, Polarization: Measurement, Analysis, and Remote Sensing XIII,

2018, 1065506

23. Wang B, Oakberg T C. A new instrument for measuring both the magnitude and angle of low level linear birefringence. Review of Scientific Instruments, 1999, 70(10): 3847–3854
24. Pham T T H, Lo Y L. Extraction of effective parameters of turbid media utilizing the Mueller matrix approach: Study of glucose sensing. Journal of Biomedical Optics, 2012, 17(9): 097002
25. Manhas S, Swami M, Buddhiwant P, et al. Mueller matrix approach for determination of optical rotation in chiral turbid media in backscattering geometry. Optics Express, 2006, 14(1): 190–202
26. Liu X, Chen X, Li Z. Modular design of typical rigid links in parallel kinematic machines: Classification and topology optimization. Frontiers of Mechanical Engineering, 2012, 7(2): 199–209
27. Zhang S, Gu H, Liu J, et al. Characterization of beam splitters in the calibration of a six-channel Stokes polarimeter. Journal of Optics, 2018, 20(12): 125606
28. Zhang S, Chen C, Jiang H, et al. Dynamic characteristics of nematic liquid crystal variable retarders (LCVRs) investigated by a high-speed polarimetry. Journal of Optics, 2019, 21(6): 065605
29. Liu J, Zhang C, Zhong Z, et al. Measurement configuration optimization for dynamic metrology using Stokes polarimetry. Measurement Science & Technology, 2018, 29(5): 054010
30. De Martino A, Kim Y K, Garcia-Caurel E, et al. Optimized Mueller polarimeter with liquid crystals. Optics Letters, 2003, 28(8): 616–618
31. Smith M H. Optimization of a dual-rotating-retarder Mueller matrix polarimeter. Applied Optics, 2002, 41(13): 2488–2493
32. Duan L, Zhang L, Wang Z. De-noising of diesel vibration signal using wavelet packet and singular value decomposition. Frontiers of Mechanical Engineering, 2006, 1(4): 443–447